Vrije Universiteit Brussel

Scaling laws for motor-gearbox arrangements

Saerens, Elias; Crispel, Stein; Lopez Garcia, Pablo; Ducastel, Vincent; Beckers, Jarl; De Winter, Joris; Furnémont, Raphaël Guy; Vanderborght, Bram; Verstraten, Tom; Lefeber, Dirk

Scaling laws for parallel motor-gearbox arrangements

Elias Saerens*, Stein Crispel, Pablo López García, Vincent Ducastel, Jarl Beckers,
Joris De Winter, Raphaël Furnémont, Bram Vanderborght, Tom Verstraten and Dirk Lefeber

Abstract— Research towards (compliant) actuators, especially redundant ones like the Series Parallel Elastic Actuator (SPEA), has led to the development of drive trains, which have demonstrated to increase efficiency, torque-to-mass-ratio, power-to-mass ratio, etc. In the field of robotics such drive trains can be implemented, enabling technological improvements like safe, adaptable and energy-efficient robots. The choice of the used motor and transmission system, as well as the compliant elements composing the drive train, are highly dependent of the application and more specifically on the allowable weight and size. In order to optimally design an actuator adapted to the desired characteristics and the available space, scaling laws governing the specific actuator can simplify and enhance the reliability of the design process. Although scaling laws of electric motors and links are known, none have been investigated for a complete redundant drive train. The present study proposes to fill this gap by providing scaling laws for electric motors in combination with their transmission system. These laws are extended towards parallelization, i.e. replacing one big motor with gearbox by several smaller ones in parallel. The results of this study show that the torque/mass ratio for a motor-gearbox can not be increased by parallelization, but that it can increase the torque/volume ratio. This is however only the case if a good topology is chosen.

I. INTRODUCTION

Compliant actuators are actuators incorporating one or more compliant elements. These actuators benefit from the inherent characteristics of their compliant elements, e.g. shock absorption and energy storage. These last two characteristics are particularly important in novel robotic applications, like exo-skeletons, prosthetics or co-bots, which require actuators with high efficiency, torque-to-mass ratio, power-to-mass ratio and a safe Human-Robot-Interaction (HRI).

While traditional stiff actuators offer superior position tracking, the aforementioned requirements are however hard to meet with such actuators [1]. This explains why compliant actuation has been a growing field in robotics for the last two decades.

Starting from the developments of Pratt et al. around Series Elastic Actuators [2] (which are compliant actuators with a fixed mechanical stiffness), several SEA designs have been optimized in order to achieve minimum mass for a maximum output torque and power, while also remaining compact. The optimization of these designs relates to the motor, transmissions (e.g. gearbox, belt,...), the compliant element and the structure of the actuator. This optimization process is however complex and depends on multiple variables. The choice of gear ratio, for example, can affect the working range of the motor, which on its turn will allow only springs with a limited range of stiffness/elongation or energy density to be used for a predefined load case. Because of this coupling, a wrong selection in one component, can influence another component in an unexpected way, which can lead to the development of an actuator with undesired output characteristics.

Furthermore, there is a trend in robotic research towards more complex actuators consisting of multiple springs and geared motors. Advantages of such concepts include increased energy efficiency [3–5], fault-tolerance, impedance [6] and accuracy [7]. However, the usefulness of the additional components must be evaluated against the total weight and volume of the system. This is a very challenging matter, since changes in the sizing of one component will inevitably affect the performance of all other components. As a result, the optimization of such complex actuators becomes an iterative process.

Indeed, the dynamics of the system can only be completely derived after selecting all components, but the whole system dynamics need to be known in the first place to make a smart choice for the components. Hence, it would be desirable to determine how certain output characteristics behave, i.e. scale, under influence of standard component characteristics, like e.g. dimensions, such that the optimization process can be simplified. In the case of a compliant actuator, such scaling laws should be derived for both motor, transmission system and compliant element in order to easily perform a multi-parameter optimization. Here we assume an electric motor, since they provide one of the highest efficiencies, while being rather compact, which is a desirable feature for the field of robotics [8].

Several works in literature already address the scaling and optimal selection of drivetrain components. Regarding motors, one of the most basic models by Marden et al. [9], [10] started deriving scaling laws by looking to the link between biology and motors. Similarities in the latter led to the discovery of a relationship between output force

and mass. Dermitzakis et al. [11] went deeper into this by searching a scaling relationship between motor torque and mass, which led to the finding that there is a limit to the possible specific torque in motors.

In order to reach this maximum torque limit, Reichert et al. [12] introduced a way to use scaling laws, such that the distinction between the performance of permanent magnet machines with interior or exterior rotor can be seen. Like this the output torque of permanent magnet machines could be maximized.

To make the optimal selection proces of actuators more realistic, Roos et al. [13] introduced non-idealities like Joule losses, inertia and both mechanical and energy efficiency as an optimization tool to select the right actuator components. A similar but improved method for such kind of optimization was presented by Giberti et al. [14–16]. In his work an 'Accelerating factor' was defined to give each motor a representative performance score. This was then also coupled to a certain 'Load factor' to see the influence on the loading condition. The concept of this 'accelerating factor' was then later improved in [17] by coupling it to the actual motor dimensions, which allowed to come closer to a scaling law and perform the multi-parameter optimization.

Rezazadeh et al. [18] studied the efficiency of a geared motor, with a focus on improving the energy efficiency of the motor by selecting the optimal transmission ratio. By doing so, the motor can work in its optimal range. This selection is done analytically by considering a transmission that has a constant efficiency for each load case and considers for the motor only Joule losses.

These motor models were expanded by Verstraten et al. [19], [20] by adding the viscous losses and the gearing in the optimal selection. They analyzed the load- and speed dependent losses together with the drive inertia, the directional efficiency of a gearbox and even the power consumption of the controller. In order to analyze the efficiency of the selected solution, Verstraten et al. also proposed the use of motor efficiency maps.

Bartlett et al. [21] dug deeper into the transmission itself, more specifically the multiple-stage gearboxes. There, an analysis is performed on how some design parameters, like number of stages and stage ratios, influence the total mechanical efficiency, mass and acceleration. This way, they aim to find the best trade-off between competing gearbox characteristics. [22].

In these gearboxes a contribution was also delivered by Pott [23], who derived how the torque and mechanical power scale as a function of a general dimensional unit 's'. The downside of this method is however that in such a way no distinction can be made between the effect of a diameter or length change, which can potentially be important for certain applications.

Caprari et al. [24] have a slightly different approach and start from the importance of the energy source in the design of actuators. They looked into the scaling laws of motor units together with possible energy sources in order to construct a micro-robot that has predefined output characteristics. This scaling however also uses a general dimensional unit, which presents the same issues as mentioned in the previous paragraph. A nice feature of their work is that they also made an analysis of the autonomy of different energy sources, which is especially important for mobile applications.

In Budinger et al. [25] one of the most extensive actuator scaling laws can be found, for each possible component, even bearings. However, they do not use a fixed parameter to scale by.

Considering the compliant elements, several studies address the optimal selection of compliant elements for mass reduction. These studies are generally based on constrained optimization, where the spring is designed in order to match the motion in order to minimize the power consumption. This is for example done by Verstraten et al. [26], [27]. Here however, the characteristics and scaling of compliant elements (i.e. springs) will be tackled in a more general manner.

Looking into all these separate components shows that several parameters can be influenced, without immediately understanding their effect on the characteristics of the output, more specifically weight and size.

In this paper we will start the study of the multi-parameter optimization problem for compliant drive trains by fining correct scaling laws for motors as a function of their basic dimensions, which can easily be found in catalogs. They will also be coupled together with the scaling laws of a planetary gear train (PGT) transmission in order to see the influence of parallelization for a rigid actuator (motor-transmission). This work can be a first step to enlighten and improve the design process of e.g. (compliant) actuators in robotics and assess the potential of novel, complex actuator technologies which incorporate a large number of components.

The layout of the paper is as follows. In section II a state of the art will be shown for the scaling laws of motors. The laws that are found will be verified against catalog data from Emoteq and MOOG and the most correct one among them will be selected. Afterwards, in section III the chosen law will be expanded in order to see the influence of changing one big motor by several smaller ones, i.e. parallelization. Once done the parallelized motor laws will be coupled to the ones of a transmission to see how T/m and T/V behave for the parallelization of a complete actuator. To finish, a conclusion and some future work will be discussed in section IV.

II. SCALING FOR MOTORS

Although many studies deal with the scaling of electric motors, only a few are consistent with existing motor data.

In this section, two different approaches are analyzed: the scaling laws derived by MIT researchers [28], [29] and by Haddadin et al. [30]. We discuss their results and compare them to data derived from the Emoteq HT Series [31] or the MOOG matrix series [32]. In this section, the parameters which are involved in the scaling law calculations, are summarized in Table I.

Symbol	Explanation	Unit
r_{gap}	Gap radius	m
k_t	Motor torque constant	Nm/A
I	Motor current	A
R	Armature resistance	Ω
n	Number of wires in the cross-section	/
H	Magnetic Field strength	A/m
m_m	Motor mass	kg
J_m	Motor inertia	$kg \cdot m^2$
r_a	Armature radius	m
l_a	Rotor length	m
r_m	Motor radius	m
l_m	Motor length	m
ρ_a	Armature density	kg/m^3
N	Reduction ratio	/
C	Utilization factor of the machine	N
B_e	Air gap flux density	Nm/A
α	Pole coverage factor	/
A	Linear current density	A/m
w_a	Number of armature winding turns	/
T_{stall}	Stall torque	Nm
ρ_w	Specific winding resistance	Ωm
l_w	Total length of the winding	m
r_w	Winding radius	m
A_w	Winding cross-section	m^2
t_s	Stator thickness	m
t_r	Rotor thickness	m
d_m	Motor diameter	m

TABLE I: Nomenclature of general motor parameters.

A. State of the art in motor scaling

1) Motor scaling according to MIT: Seok et al. [28], [29] scale motors based on the gap radius r_{gap}, which they define as the distance from the motor's axis to the center of the gap between the permanent magnets and the rotor. The motor mass, motor stall torque and motor inertia are related to this r_{gap} as:

$$\begin{cases} m_m & \propto r_{gap} \\ T_{stall} & \propto r_{gap}^2 \\ J_m & \propto r_{gap}^3 \end{cases} \quad (1)$$

Furthermore, all these values scale linearly with the length of the motor l_m. Based on these equations, the torque density is given by:

$$\frac{T_{stall}}{m_m} \propto r_{gap} \quad (2)$$

The acceleration capability is given by:

$$\frac{T_{stall}}{J_m} \propto r_{gap}^{-1} \quad (3)$$

The torque production efficiency is given by:

$$\frac{k_t^2}{R} = \frac{T_{stall}^2}{RI^2} \propto \frac{nl_m HA_w}{\rho_w}r_{gap}^2 \quad (4)$$

Given a particular wire gauge, the number of wires in the cross section (n) scales linearly with the gap radius of the motor. As result we get:

$$\frac{k_t^2}{R} \propto r_{gap}^3 \quad (5)$$

Comparing these theoretical values to the scaling of real motor data (Fig. 1) reveals that this prediction is not very accurate.
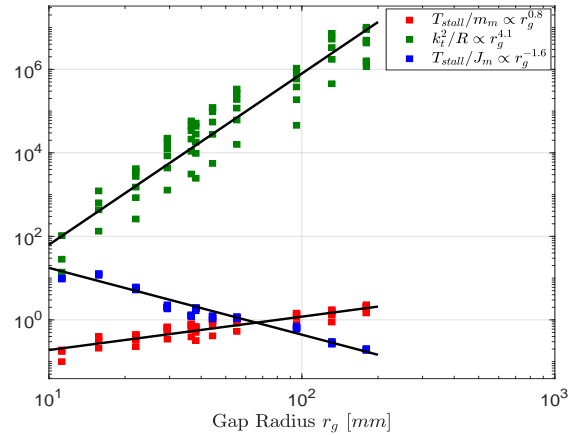

Fig. 1: Motor performance metrics T_{stall}/J_m, T_{stall}/m_m, and k_t^2/R in function of the gap radius (r_g). The displayed data points are extracted from Emoteq frameless HT series motors [31]. The black lines represent the scaling trend mentioned in the legend for each motor performance metric.

In Fig. 1 it can be seen that for the chosen data, the torque density is proportional to $r_g^{0.8}$, the acceleration capability is proportional to $r_g^{-1.6}$ and the torque production efficiency is proportional to $r_g^{4.1}$. In comparison: the theoretical factors of proportionality are r_g^1, r_g^{-1} and r_g^3, respectively from (2),(3) and (5).

The fact that this scaling is not entirely correct is due to some assumptions made by the authors which are not completely valid. They make the assumption that the motors have a constant stator and rotor thickness, whereas for the Emoteq HT series motors, the stator and rotor thicknesses scale by [29]:

$$\begin{cases} t_s \propto r_g^{0.8} \\ t_r \propto r_g^{0.4} \end{cases}$$

Implementing this would lead to an increase in the torque production efficiency and a decrease in torque density and acceleration capability. This trend can indeed be seen for the catalog data in Fig. 1.

However, since changing the rotor/stator thickness has a nonlinear effect on the magnitude of the magnetic field at the rotor-stator air gap, and heavily influences stator winding design, it is difficult to model these changes accurately [29]. Because of this, the authors deliberately only considered a fixed rotor and stator thickness, in order to facilitate the scaling model.

2) Motor scaling according to Haddadin: In Haddadin et al. [30], the equations are derived in a different way.

The maximum torque (stall torque) is calculated as follows:

$$T_{stall} = 2\pi C l_m r_m^2 \qquad (6)$$

Here C is the utilization factor of the machine, given by:

$$C = \pi^2 \alpha A B_e \qquad (7)$$

This utilization factor contains also the linear current density A, which can be written as:

$$A = \frac{w_a I}{2\pi r_a} \qquad (8)$$

The linear current density scales with the armature radius as:

$$A \propto \sqrt{r_a} \qquad (9)$$

Assuming constant α, saturated flux density and a bore volume proportional with the volume of the motor (r_a and l_a proportional with r_m and l_m). This assumption can be made, since not the stator size itself, but the provided air-gap flux influences the dynamic performance of the machine [30].

Considering these assumptions, we obtain that the stall torque scales as:

$$T_{stall} \propto l_m r_m^{5/2} \qquad (10)$$

From Eqs. (8) and (9), we find that the current scales as:

$$I \propto r_a^{3/2} \qquad (11)$$

For the armature winding resistance R, we have then:

$$R = \frac{\rho_w l_w}{A_w} = 2\rho_w \frac{w_a(r_a + l_a)}{\pi r_w^2} \qquad (12)$$

Where the winding cross-section is given by $A_w = \pi r_w^2$.

If we keep the numbers of wires constant, but assume that the diameter of the wires is proportional to the armature radius, we can then obtain:

$$R \propto \frac{(2r_a + l_a)}{\pi r_a^2} \qquad (13)$$

Now, to derive the motor metrics, first the scaling of mass and inertia need to be derived. The motor mass is given by:

$$m_m = \rho_m l_m r_m^2 \pi \qquad (14)$$

When considering again r_a and l_a proportional with r_m and l_m, the following relationship for the torque density can be found:

$$\frac{T_{stall}}{m_m} \propto \frac{l_m r_m^{5/2}}{\pi \rho_m l_m r_m^2} \propto r_m^{1/2} \qquad (15)$$

And, since the inertia is calculated as:

$$J_m = \frac{1}{2}\pi \rho_a l_a r_a^4 N^2 \qquad (16)$$

The acceleration capability can be written as:

$$\frac{T_{stall}}{J_m} \propto \frac{l_m r_m^{5/2}}{\frac{1}{2}\pi \rho_m l_m r_m^4} \propto r_m^{-3/2} \qquad (17)$$

To validate these metrics, the torque density and acceleration capability of the Emoteq frameless HT series motors are plotted in function of their diameter (which is valid, since $d_m \propto r_m$). This plot can be seen in Fig. 2.
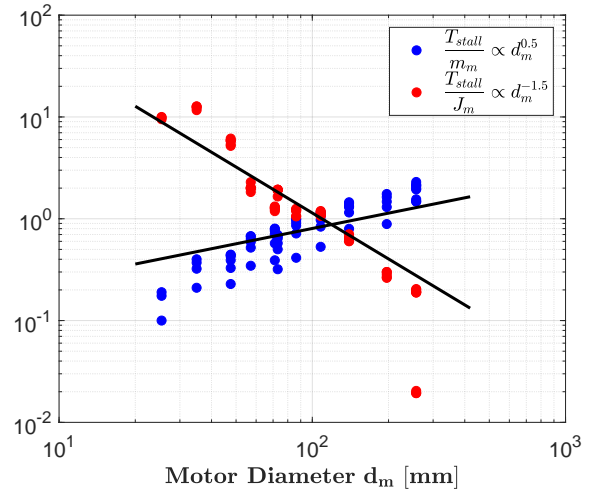

Fig. 2: Motor performance metrics T_{stall}/m_m and T_{stall}/J_m in function of the motor diameter (d_m). The displayed data points are extracted from Emoteq frameless HT series motors [31]. The black lines represent the scaling trend mentioned in the legend for each motor performance metric.

From Fig. 2 it can be observed that the derived laws respectively from (15) and (17) follow rather good the catalog data. The deviations arise from the assumptions made, which is especially visible for the plot of $\frac{T_{stall}}{m_m}$, since there T_{stall} is related to the armature dimensions, whereas the mass is related to the outside motor dimensions. For the plot of $\frac{T_{stall}}{J_m}$ the deviation is less visible, since both the torque and inertia are based on the armature parameters and hence the transition from armature to motor parameters is eliminated by the division.

We can also try to find the torque production efficiency:

$$\frac{k_t^2}{R} = \frac{T_{stall}^2}{RI^2} \propto \frac{l_m^2 r_m^5}{(2r_m+l_m)r_m^{-2}r_m^3} \propto \frac{l_m^2 r_m^4}{(2r_m+l_m)} \quad (18)$$

For long motors, this becomes:

$$\frac{k_t^2}{R} \propto l_m r_m^4 \quad (19)$$

On the other hand, for short, high-radius motors, the torque production efficiency scales as:

$$\frac{k_t^2}{R} \propto l_m^2 r_m^3 \quad (20)$$

To see how they behave in comparison with catalog data, also for the torque production efficiency a plot is made (see Fig. 3)
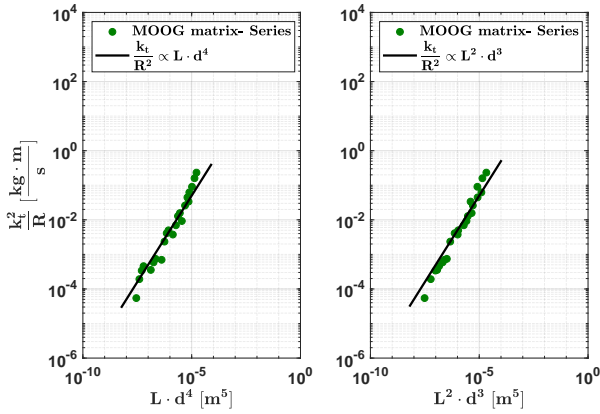

Fig. 3: Motor performance metric k_t^2/R in function of the motor diameter and length (d_m and l_m) for long motors (left) and for short, high-radius motors (right). The displayed data points are extracted from MOOG Matrix series motors [32]. The black lines represent the scaling trend mentioned in the legend.

We can conclude that, in terms of acceleration capability and torque production efficiency (formula for long motors), the equations derived from [30] give a much better representation of reality than MIT's work. Torque density is reasonably accurate for both.

III. PARALLELIZATION OF MOTOR-TRANSMISSION ARRANGEMENT

Now that it is verified which one of the scaling laws of motors gives the best representation of the reality and is the easiest to use in the design process, the laws can be extended to see the influence of parallelization, i.e. replacing one big motor by multiple smaller ones that in total still give the same output. In this section this parallelization will be done for both motor and transmission, such that the effect on the total mass and volume can then be verified for a complete rigid actuator, i.e. motor-transmission coupling.

A. Parallelization of motors

To start, the scaling law of the motor torque will be used:

$$T_m \propto Ld^{5/2} \quad (21)$$

For this parallelization study, we will assume that the length remains unchanged, however the torque necessary for each motor will be divided by the amount of parallel units, n. Applying this for one motor gives that:

$$T_{m,n} = \frac{T_m}{n} \propto \frac{Ld^{5/2}}{n} = Ld_n^{5/2} \quad (22)$$

In this equation, the relationship between d_n and d needs to be found. Hence, if we consider that the length stays equal, the expression for the motor diameter as a function of the number of parallel units and the initial diameter, becomes:

$$d_n = dn^{-2/5} \quad (23)$$

B. Parallelization of transmissions

If now a transmission would be coupled to the motor, the scaling laws of these transmission need to be known. These are given by [33]:

$$T_{PGT} \quad \propto \frac{L \cdot d^2}{a} \quad \text{if Planetary Gear Train} \quad (24)$$

$$T_{HD} \quad \propto d^3 \quad \text{if Harmonic Drive} \quad (25)$$

$$T_{CD} \quad \propto \frac{d^4}{L} \quad \text{if Cycloid Drive} \quad (26)$$

Here a represents the number of stages. To proceed it will be assumed that we will work with a planetary gear train (PGT), since this is the most common.

Combining this with the fact that for parallelization the required torque for each of the transmissions will also be divided by n, the following expression can be written:

$$T_{PGT,n} = \frac{T_{PGT}}{n} \propto \frac{Ld^2}{n \cdot a} = \frac{L_n d_n^2}{a} \quad (27)$$

For the design of this PGT it will be chosen to fit radially perfectly to the used motor. This involves that also for the PGT Eq. (23) is valid. Hence, only the expression for the PGT length as a function of the number of parallel units and the initial length needs to be still found. By combining Eqs. (23) and (27) it can be found that:

$$L_n = L \cdot n^{-1/5} \quad (28)$$

With all these equations found, it can finally be concluded how the parallelization will effect the mass and size of a motor-PGT coupling.

C. Effects of parallelization on the mass and volume for a Motor-PGT arrangement

To define the effects of parallelization on mass and volume, the definitions used in [34] will be used, namely that:

$$\begin{cases} O(m) & = \frac{m(N)}{m(N=1)} \\ O(V) & = \frac{V(N)}{V(N=1)} \end{cases}$$

1) Effect on the mass: First the effects on the mass will be investigated and this initially for the motor and *PGT* separately:

$$\begin{cases} O_{motor}(m) = \frac{n \cdot d_n^2 \cdot L_{m,n}}{d^2 \cdot L_m} = \frac{n \cdot d^2 \cdot n^{-4/5} \cdot L_m}{d^2 \cdot L_m} = n^{1/5} \\ O_{PGT}(m) = \frac{n \cdot d_n^2 \cdot L_{PGT,n}}{d^2 \cdot L_{PGT}} = \frac{n \cdot d^2 \cdot n^{-4/5} \cdot L_{PGT} \cdot n^{-1/5}}{d^2 \cdot L_{PGT}} = 1 \end{cases} \quad (29)$$

Here it can already be concluded that in terms of mass optimization, parallelization is never a good thing to do.

When coupling them together, the following can be found:

$$O_{total}(m) = \frac{n \cdot d_n^2 \cdot (L_{m,n} + L_{PGT,n})}{d^2 \cdot (L_m + L_{PGT})} = \frac{\left(\frac{L_m}{L_{PGT}}\right) \cdot n^{1/5} + 1}{\left(\frac{L_m}{L_{PGT}}\right) + 1} \quad (30)$$

This result shows that the final result depends on the ratio between the length of the motor vs. the one of the *PGT*, which is usually an indication on the type of motor that is used. If the motor is rather short in comparison with the coupled transmission, it leans more towards a high torque motor. In the other case it leans more towards a high speed motor.

In Fig. 4 the influence of parallelization is shown for the mass for both the motor-PGT coupling as for the individual components.

From this figure it can be seen that all possible motor-PGT couplings can be found between the extreme cases of the motor and *PGT* individually, which were derived in Eq. (29). Hence it can be concluded that also for the coupling, parallelization is never beneficial in terms of mass optimization. The interesting conclusion can however be made here that high torque motors lose less in the parallelization process than their high speed counterparts.

2) Effect on the volume: When looking to the volume, the derivation is not as straightforward as for the mass, since a lot depends on the packing of the different motor-PGT couplings. To show this, the effect of parallelization will be shown for two different types of packings, namely circular packing and side-to-side packing. For both cases not the complete derivation will be done, but the expression for the parallelized volume and the $O(V)$ of the individual components and the total motor-PGT coupling will be given.

- **Circular packing**
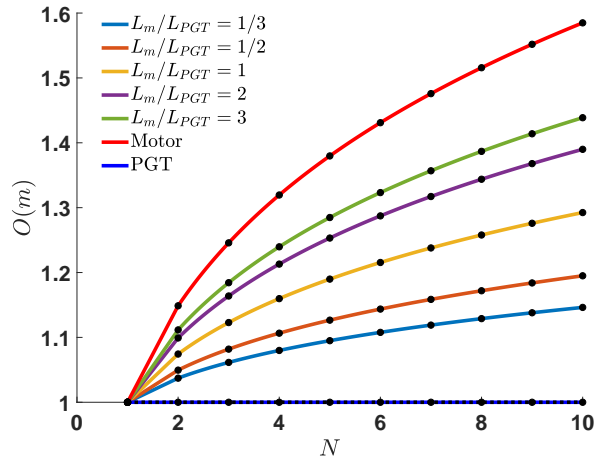 The circular packing is defined as shown in Fig. 5

Fig. 4: Effect of parallelization on the total mass. This effect is shown for the parallelization of a motor (red line), a planetary gear train (*PGT*) (dark blue line) and motor-PGT couplings with different length distributions. In this graph N represents the degree of parallelization. It can be seen that for mass reduction, parallelization is never useful.
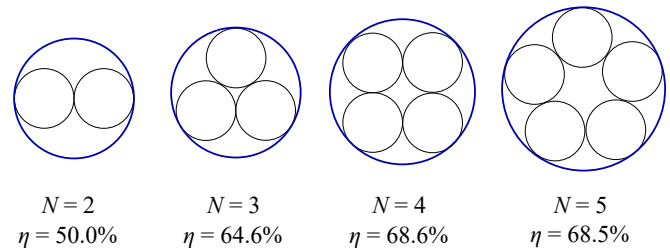

Fig. 5: Representation of the circular packing topology as a function of the used parallelization number, also the packing efficiency is indicated for each parallelization number.

This topology leads to a parallelized volume, like expressed in Eq. (31) and gives volume scaling equations which are shown in Eq. (32). The results from this parallelization are shown in Fig. 6.

$$V(N) = d_n^2 \cdot L_n \cdot \left(1 + \frac{1}{sin(\frac{\pi}{n})}\right)^2 \quad (31)$$

$$\begin{cases} O_{motor}(V) = n^{-4/5} \cdot \left(1 + \frac{1}{sin(\frac{\pi}{n})}\right)^2 \\ O_{PGT}(V) = n^{-1} \cdot \left(1 + \frac{1}{sin(\frac{\pi}{n})}\right)^2 \\ O_{total}(V) = O_{motor}(V) \cdot \left(\frac{\frac{L_m}{L_{PGT}} + n^{-1/5}}{\frac{L_m}{L_{PGT}} + 1}\right) \end{cases} \quad (32)$$

- **Side-to-side packing**
  The side-to-side packing, which can e.g. be found in [35], is defined as shown in Fig. 7
  This topology leads to a parallelized volume, like expressed in Eq. (33) and gives volume scaling equations
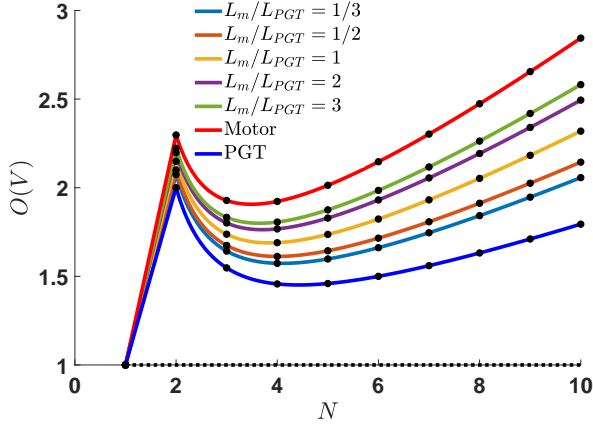
Fig. 6: Effect of parallelization on the total volume for a circular packing topology. This effect is shown for the parallelization of a motor (red line), a planetary gear train (PGT) (dark blue line) and motor-PGT couplings with different length distributions. In this graph N represents the degree of parallelization. It can be seen that when a circular packing topology is used, parallelization will never reduce the total volume.

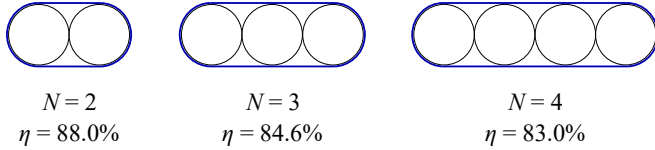| $N = 2$ | $N = 3$ | $N = 4$ |
| $\eta = 88.0\%$ | $\eta = 84.6\%$ | $\eta = 83.0\%$ |

Fig. 7: Representation of the side-to-side packing topology as a function of the used parallelization number, also the packing efficiency is indicated for each parallelization number.
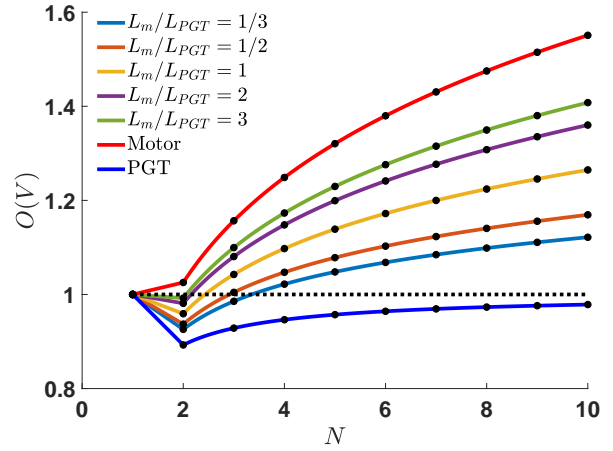

Fig. 8: Effect of parallelization on the total volume for a side-to-side packing topology. This effect is shown for the parallelization of a motor (red line), a planetary gear train (PGT) (dark blue line) and motor-PGT couplings with different length distributions. In this graph N represents the degree of parallelization. It can be seen that when a side-to-side packing topology is used, parallelization can in some cases reduce the total volume, especially for $N = 2$. For values higher than $N = 3$ there will however be no volume reduction anymore.

which are shown in Eq. (34). The results from this parallelization are shown in Fig. 8.

$$V(N) = L_n \cdot \left((n-1) \cdot d_n^2 + \frac{d_n^2 \pi}{4} \right) \qquad (33)$$

$$\begin{cases} O_{motor}(V) = n^{-4/5} \cdot \left(\frac{\pi}{4} - 1 \right) + n^{1/5} \\ O_{PGT}(V) = n^{-1} \cdot \left(\frac{\pi}{4} - 1 \right) + 1 \\ O_{total}(V) = O_{motor}(V) \cdot \left(\frac{\frac{L_m}{L_{PGT}} + n^{-1/5}}{\frac{L_m}{L_{PGT}} + 1} \right) \end{cases} \qquad (34)$$

From Figs. 6 and 8 it can be concluded that the packing topology is crucial in whether the volume can be optimized due to parallelization or not. In the case of Fig. 6 rather low packing efficiencies are noted, with a minimum of 50% at $N = 2$, which can clearly be seen. Due to this, a circular packing topology will never result in an optimization of T/V. However, in Fig. 8 T/V can be optimized due to parallelization, since that topology has a rather high packing efficiency, with a maximum of 88% at $N = 2$. It is due to this high efficiency that different motor-PGT couplings show to have a decreased total volume for $N = 2$.

It is also interesting to note that each of the possible actuator values lies between the extremities of the motor and PGT individually.

IV. CONCLUSION

In this paper the state of the art in scaling laws for motors is compared and verified with catalog data. Based on this, the best law is chosen and then extended to see the effect of parallelization for both total mass and volume. This is then coupled to the scaling laws of transmissions in order to verify the effect of parallelization on a rigid actuator, i.e. a motor-transmission coupling. From this analysis it is concluded that splitting up one big actuator into multiple smaller ones is never useful if T/m needs to be increased, but that it can be useful if the objective is to optimize T/V. It is however noted that the way of packing the multiple parallel units plays a very important role in whether parallelization is positive or not.

Future work will be pointed towards implementing these scaling laws for compliant actuators, as well as finding an answer to optimize T/J. Like this the design process of (compliant) redundant actuators could be hugely simplified.

REFERENCES

[1] R. v. Ham, T. Sugar, B. Vanderborght, K. Hollander, and D. Lefeber, "Compliant actuator designs," *IEEE Robotics & Automation Magazine*, vol. 3, no. 16, pp. 81–94, 2009.

[2] G. A. Pratt and M. M. Williamson, "Series elastic actuators," in *Proceedings 1995 IEEE/RSJ International Conference on Intelligent Robots and Systems. Human Robot Interaction and Cooperative Robots*, vol. 1. IEEE, 1995, pp. 399–406.

[3] T. Verstraten, G. Mathijssen, R. Furnémont, B. Vanderborght, and D. Lefeber, "Modeling and design of geared dc motors for energy efficiency: Comparison between theory and experiments," *Mechatronics*, vol. 30, pp. 198–213, 2015.

[4] G. Mathijssen, R. Furnémont, T. Verstraten, C. Espinoza, S. Beckers, D. Lefeber, and B. Vanderborght, "Study on electric energy consumed in intermittent series–parallel elastic actuators (ispea)," *Bioinspiration & biomimetics*, vol. 12, no. 3, p. 036008, 2017.

[5] T. Verstraten, J. Geeroms, G. Mathijssen, B. Convens, B. Vanderborght, and D. Lefeber, "Optimizing the power and energy consumption of powered prosthetic ankles with series and parallel elasticity," *Mechanism and Machine Theory*, vol. 116, pp. 419–432, 2017.

[6] B.-S. Kim, J.-B. Song, and J.-J. Park, "A serial-type dual actuator unit with planetary gear train: Basic design and applications," *IEEE/ASME Transactions on Mechatronics*, vol. 15, no. 1, pp. 108–116, 2009.

[7] J. Ontañón-Ruiz, R. Daniel, and P. Mcree, "On the use of differential drives for overcoming transmission nonlinearities," *Journal of Robotic Systems*, vol. 15, no. 11, pp. 641–660, 1998.

[8] J. D. Madden, "Mobile robots: motor challenges and materials solutions," *science*, vol. 318, no. 5853, pp. 1094–1097, 2007.

[9] J. H. Marden and L. R. Allen, "Molecules, muscles, and machines: universal performance characteristics of motors," *Proceedings of the National Academy of Sciences*, vol. 99, no. 7, pp. 4161–4166, 2002.

[10] J. H. Marden, "Scaling of maximum net force output by motors used for locomotion," *Journal of Experimental Biology*, vol. 208, no. 9, pp. 1653–1664, 2005.

[11] K. Dermitzakis, J. P. Carbajal, and J. H. Marden, "Scaling laws in robotics," *Procedia Computer Science*, vol. 7, pp. 250–252, 2011.

[12] T. Reichert, T. Nussbaumer, and J. W. Kolar, "Torque scaling laws for interior and exterior rotor permanent magnet machines," *A A*, vol. 3, p. 1, 2009.

[13] F. Roos, H. Johansson, and J. Wikander, "Optimal selection of motor and gearhead in mechatronic applications," *Mechatronics*, vol. 16, no. 1, pp. 63–72, 2006.

[14] H. Giberti, S. Cinquemani, and G. Legnani, "Effects of transmission mechanical characteristics on the choice of a motor-reducer," *Mechatronics*, vol. 20, no. 5, pp. 604–610, 2010.

[15] ——, "A practical approach to the selection of the motor-reducer unit in electric drive systems," *Mechanics based design of structures and machines*, vol. 39, no. 3, pp. 303–319, 2011.

[16] H. Giberti and S. Cinquemani, "Servo motors classification based on the accelerating factor," in *3rd International Multi-Conference on Engineering and Technological Innovation (IMETI 2010)*, 2010, pp. 1–7.

[17] H. Giberti, A. Clerici, and S. Cinquemani, "Specific accelerating factor: One more tool in motor sizing projects," *Mechatronics*, vol. 24, no. 7, pp. 898–905, 2014.

[18] S. Rezazadeh and J. W. Hurst, "On the optimal selection of motors and transmissions for electromechanical and robotic systems," in *2014 IEEE/RSJ international conference on intelligent robots and systems*. IEEE, 2014, pp. 4605–4611.

[19] T. Verstraten, G. Mathijssen, R. Furnémont, B. Vanderborght, and D. Lefeber, "Modeling and design of geared dc motors for energy efficiency: Comparison between theory and experiments," *Mechatronics*, vol. 30, pp. 198–213, 2015.

[20] T. Verstraten, R. Furnémont, G. Mathijssen, B. Vanderborght, and D. Lefeber, "Energy consumption of geared dc motors in dynamic applications: Comparing modeling approaches," *IEEE Robotics and Automation Letters*, vol. 1, no. 1, pp. 524–530, 2016.

[21] H. L. Bartlett, B. E. Lawson, and M. Goldfarb, "On the design of power gear trains: Insight regarding number of stages and their respective ratios," *PloS one*, vol. 13, no. 6, 2018.

[22] A. Wang and S. Kim, "Directional efficiency in geared transmissions: Characterization of backdrivability towards improved proprioceptive control," in *2015 IEEE International Conference on Robotics and Automation (ICRA)*. IEEE, 2015, pp. 1055–1062.

[23] P. P. Pott, "Entwurfskriterien feinwerktechnischer integrierter sensor-aktor-systeme," 2015.

[24] G. Caprari, T. Estier, and R. Siegwart, "Fascination of down scaling-alice the sugar cube robot," Tech. Rep., 2000.

[25] M. Budinger, J. Liscouët, F. Hospital, and J. Maré, "Estimation models for the preliminary design of electromechanical actuators," *Proceedings of the Institution of Mechanical Engineers, Part G: Journal of Aerospace Engineering*, vol. 226, no. 3, pp. 243–259, 2012.

[26] R. Nasiri, M. Khoramshahi, M. Shushtari, and M. N. Ahmadabadi, "Adaptation in variable parallel compliance: Towards energy efficiency in cyclic tasks," *IEEE/ASME Transactions on Mechatronics*, vol. 22, no. 2, pp. 1059–1070, 2016.

[27] T. Verstraten, P. Beckerle, R. Furnémont, G. Mathijssen, B. Vanderborght, and D. Lefeber, "Series and parallel elastic actuation: Impact of natural dynamics on power and energy consumption," *Mechanism and Machine Theory*, vol. 102, pp. 232–246, 2016.

[28] S. Seok, A. Wang, D. Otten, and S. Kim, "Actuator design for high force proprioceptive control in fast legged locomotion," in *2012 IEEE/RSJ International Conference on Intelligent Robots and Systems*. IEEE, 2012, pp. 1970–1975.

[29] P. M. Wensing, A. Wang, S. Seok, D. Otten, J. Lang, and S. Kim, "Proprioceptive actuator design in the mit cheetah: Impact mitigation and high-bandwidth physical interaction for dynamic legged robots," *IEEE Transactions on Robotics*, vol. 33, no. 3, pp. 509–522, 2017.

[30] S. Haddadin, N. Mansfeld, and A. Albu-Schäffer, "Rigid vs. elastic actuation: Requirements & performance," in *2012 IEEE/RSJ International Conference on Intelligent Robots and Systems*. IEEE, 2012, pp. 5097–5104.

[31] *High Torque Series Brushless DC Motors*. Emoteq Inc., 2018, [PDF file].

[32] *Motion Technology Catalog Brushless and Brush Motors, Drive Electronics, Gearheads and Position Sensors*. Moog Components Group, 2014, [PDF file].

[33] E. Saerens, S. Crispel, P. L. García, T. Verstraten, V. Ducastel, B. Vanderborght, and D. Lefeber, "Scaling laws for robotic transmissions," *Mechanism and Machine Theory*, vol. 140, pp. 601–621, 2019.

[34] E. Saerens, R. Furnémont, T. Verstraten, P. L. García, S. Crispel, V. Ducastel, B. Vanderborght, and D. Lefeber, "Scaling laws of compliant elements for high energy storage capacity in robotics," *Mechanism and Machine Theory*, vol. 139, pp. 482–505, 2019.

[35] G. Mathijssen, R. Furnémont, T. Verstraten, B. Brackx, J. Premec, R. Jiménez, D. Lefeber, and B. Vanderborght, "+ spea introduction: drastic actuator energy requirement reduction by symbiosis of parallel motors, springs and locking mechanisms," in *2016 IEEE International Conference on Robotics and Automation (ICRA)*. IEEE, 2016, pp. 676–681.